Repulsive Fermi Polarons in a Resonant Mixture of Ultracold ^{6}Li Atoms

F. Scazza,[1,2,*] G. Valtolina,[1,2] P. Massignan,[3] A. Recati,[4,5] A. Amico,[2] A. Burchianti,[1,2] C. Fort,[2] M. Inguscio,[1,2] M. Zaccanti,[1,2] and G. Roati[1,2]

[1]*Istituto Nazionale di Ottica del Consiglio Nazionale delle Ricerche (INO-CNR), 50019 Sesto Fiorentino, Italy*
[2]*LENS and Dipartimento di Fisica e Astronomia, Università di Firenze, 50019 Sesto Fiorentino, Italy*
[3]*ICFO-Institut de Ciencies Fotoniques, The Barcelona Institute of Science and Technology, 08860 Castelldefels, Spain*
[4]*INO-CNR BEC Center and Dipartimento di Fisica, Università di Trento, 38123 Povo, Italy*
[5]*Ludwig-Maximilians-Universität München, 80333 München, Germany*

(Received 30 September 2016; published 21 February 2017)

We employ radio-frequency spectroscopy to investigate a polarized spin mixture of ultracold ^{6}Li atoms close to a broad Feshbach scattering resonance. Focusing on the regime of strong repulsive interactions, we observe well-defined coherent quasiparticles even for unitarity-limited interactions. We characterize the many-body system by extracting the key properties of repulsive Fermi polarons: the energy E_+, the effective mass m^*, the residue Z, and the decay rate Γ. Above a critical interaction, E_+ is found to exceed the Fermi energy of the bath, while m^* diverges and even turns negative, thereby indicating that the repulsive Fermi liquid state becomes energetically and thermodynamically unstable.

DOI: 10.1103/PhysRevLett.118.083602

Landau's idea of mapping the behavior of impurity particles interacting with a complex environment into quasiparticle properties [1] plays a fundamental role in physics and materials science, from helium liquids [2] and colossal magnetoresistive materials [3,4] to polymers and proteins [5,6]. In the field of ultracold gases, the impurity problem and the associated concept of the polaron quasiparticle have attracted over the past decade a growing interest [7–10]. Initiated with the investigation of polarized Fermi gases in the BEC-BCS crossover [11–16], the study of polaron physics has been extended to mass-imbalanced [17,18], low-dimensional fermionic systems [19] and also to bosonic environments [20–22]. The polaron properties are fundamentally relevant for understanding the more complex scenario of partially polarized and balanced Fermi mixtures: The impurity limit exhibits some of the critical points of the full phase diagram, whose topology we can thus learn about by investigating polarized systems [8,16].

While researchers initially focused on attractive interactions [14,15], more recently they have explored novel quasiparticles associated with repulsive interactions: These repulsive polarons [23–27] are centrally important for realizing repulsive many-body states [23,24,28,29] and therein exploring itinerant ferromagnetism [30–32]. In particular, if the polaron energy exceeds the Fermi energy of the surrounding medium, a fully ferromagnetic phase is favored against the paramagnetic Fermi liquid [23–25,27]. However, short-ranged strong repulsion always require an underlying weakly bound molecular state, into which the system may rapidly decay [31,33], making the repulsive polaron an excited many-body state, whose theoretical and experimental investigation are challenging. In three dimensions, repulsive Fermi polarons have been first unveiled in a ^{6}Li-^{40}K mixture at a comparatively narrow Feshbach resonance [17], but they lack observation in the universal, broad resonance case, for which the decay rate is expected to be the largest [10].

In this Letter, we report on reverse radio-frequency (rf) spectroscopy [17,34,35] experiments to unveil the existence and characterize the properties of repulsive polarons in a polarized Fermi mixture of lithium atoms, interacting at a broad Feshbach resonance. We obtain precise information about (i) the energy E_+, (ii) the effective mass m^*, and (iii) the decay rate Γ of repulsive polarons. Furthermore, we probe the coherence properties of these fermionic excitations and extract (iv) the quasiparticle residue Z. Our findings imply that phase separation is energetically allowed above a critical value of repulsion, where E_+ is found to exceed the Fermi energy of the majority atoms [23–25,27]. We also observe a negative effective mass at strong coupling, which points to a thermodynamical instability of the repulsive polaron Fermi liquid [36,37]. Unexpectedly, the measured decay rate of the repulsive branch population at the critical point is less than $0.1E_+$, and never exceeds $0.2E_+$, demonstrating the existence of well-defined repulsive quasiparticles even for resonant interactions.

In our experiment, we initially produce a weakly interacting imbalanced mixture of ^{6}Li atoms in the two lowest Zeeman states, hereafter denoted as $|1\rangle$ and $|2\rangle$, respectively, held in a crossed optical dipole trap at a bias magnetic field of 300 G [38]. The majority $|1\rangle$-component forms a highly degenerate Fermi gas with $N_1 \simeq 1.5 \times 10^5$ atoms at $T/T_F = 0.10(2)$, where $E_F = k_B T_F \simeq h \times 9.5\,\mathrm{kHz}$ is the Fermi energy and k_B and h, respectively, denote the Boltzmann and Planck constants. The state-$|1\rangle$ Fermi gas acts as a bath for the minority state-$|2\rangle$ impurities, whose concentration $x = N_2/N_1$ is finely adjusted between 0.05 and 0.4 [38]. To explore strong impurity-bath interactions, we exploit the third-to-lowest Zeeman state $|3\rangle$ and the

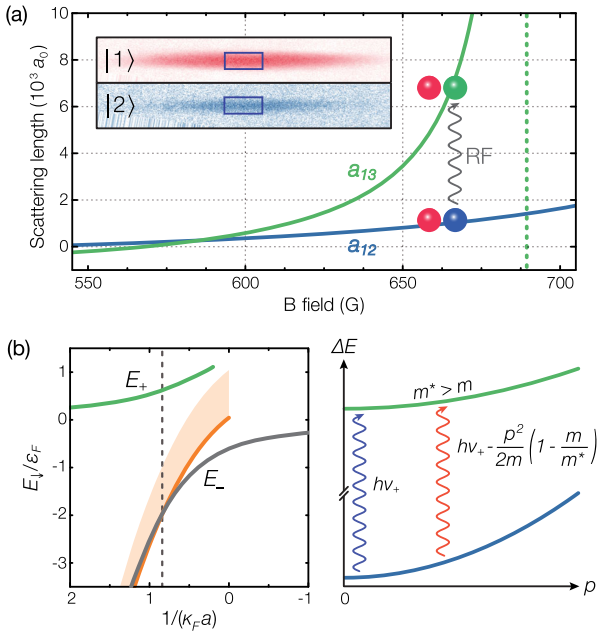

FIG. 1. (a) Scattering properties of the initial 1–2 and final 1–3 state mixtures. The rf pulse pumps impurities from the weakly interacting into the resonant state. Inset: *In situ* absorption images of the state $|1\rangle$ (red) and $|2\rangle$ (blue) atomic clouds for $x = 0.10(1)$. The rectangles mark the central region where the spectroscopy signal is recorded. (b) Left: Energy $E_\downarrow$ landscape of a zero-momentum impurity interacting with a homogeneous Fermi gas. The shaded area denotes the dressed dimer continuum, and the vertical dashed line marks the polaron-molecule crossing. Right: Sketch of the momentum dependence of the impurity resonance frequency. The blue (green) curve depicts the dispersion of bare (dressed) impurities.

tunability of the scattering lengths a_{12} and a_{13} enabled by two off-centered broad Feshbach resonances between the 1–2 and 1–3 spin combinations. Upon increasing the bias field to values between 600 and 700 G, we resonantly enhance the 1-3 scattering while moderately increasing the comparatively weak 1–2 interactions [see Fig. 1(a)].

In order to probe the full excitation spectrum of the impurities, we employ reverse rf spectroscopy [17,34,35]: We drive the $|2\rangle$ atoms on the $|2\rangle \rightarrow |3\rangle$ transition to the resonantly interacting state, using a rf pulse with variable frequency ν. Our spectroscopy signal is the transferred fraction $\mathcal{N}_3/(\mathcal{N}_2+\mathcal{N}_3)$, where $\mathcal{N}_i$ is the number of $|i\rangle$ atoms contained in a centered region of size 70 μm (30 μm) along the axial (transverse) direction of the trap [see Fig. 1(a)]. For each experimental run, the populations $\mathcal{N}_2$ and $\mathcal{N}_3$ are separately monitored by acquiring two consecutive *in situ* absorption images delayed by 500 μs. The transferred fraction is measured as a function of the rf detuning $\Delta = \nu - \nu_0$ from the frequency ν_0 of the non-interacting rf transition, measured in the absence of majority atoms. Extracting the signal from such a central region helps to reduce the effects of density inhomogeneity. The bath is characterized by effective Fermi energy $\varepsilon_F \simeq 0.74 E_F$ and wave vector $\kappa_F \simeq 0.86 k_F$, averaged over the *in situ* density distribution of the state-$|1\rangle$ gas within the integration region [38]. The bath residual inhomogeneity quantified by a standard deviation $\Delta\kappa_F \sim 0.1\kappa_F$. From here on, interactions will be parametrized by $1/(\kappa_F a) \equiv 1/(\kappa_F a_{13})$.

Figure 1(b) illustrates the generic energy spectrum of a zero-momentum impurity in a Fermi sea in the mass-balanced and broad resonance case. Attractive and repulsive polarons appear as discrete levels, with monotonically increasing energies E_+ and E_- as $1/(\kappa_F a)$ is decreased. Moreover, the repulsive polaron acquires an increasingly large width (not shown), owing to a nonzero probability to decay onto lower-lying states. These also include a broad continuum of molecular excitations of spectral width $\sim\varepsilon_F$, which arise from processes in which the impurity and any of the majority fermions are bound into a molecule. The attractive polaron enters the molecular continuum for $1/(\kappa_F a) \gtrsim 0.9$ [36,53], beyond which a dressed molecule becomes energetically favored. Reverse rf spectroscopy allows us to entirely explore this energy landscape: Besides a broad molecular state contribution, peaks in the rf signal centered at $\Delta_+ > 0$ ($\Delta_- < 0$) are identified as the repulsive (attractive) polaron states, providing access to E_+ (E_-).

Typical repulsive polaron spectra at various $1/(\kappa_F a)$ values, obtained using a 1 ms-long rectangular pulse, i.e., a 0.8π pulse for noninteracting impurity atoms, are displayed in Fig. 2(a). These are shown together with Gaussian fits employed to extract the resonance position Δ_+. The rf shift Δ_+ increases monotonically when increasing $\kappa_F a$, while the resonance progressively widens, owing mainly to collisional broadening in the final state [17,18,38]. The resonance shift reflects the increase of the polaron energy due to the repulsion between the impurities and the surrounding medium. However, the link between the measured Δ_+ and the zero-momentum polaron energy E_+ is complicated by an observed strong dependence of Δ_+ upon the impurity concentration x [see Fig. 2(b)]. This can, in principle, arise from two distinct effects. A first effect is associated to the different dispersions featured by the initial weakly interacting impurity, characterized by the bare atomic mass m, and by the final quasiparticle with effective mass m^* [see Fig. 1(b)]. Increasing x from 0 to 1 at fixed $T \simeq 0.1 T_F$, the mean motional energy per impurity in the region of interest grows nonlinearly from $\bar{\varepsilon} \simeq 0.42\varepsilon_F$ to $\bar{\varepsilon} \simeq \varepsilon_F$, due to the increased Fermi pressure of the minority gas [38]. Since the rf driving transfers the impurities into final polaron states without modifying their momentum, we expect the measured resonance shift Δ_+ at fixed $\kappa_F a$ to depend linearly upon the mean impurity energy $\bar{\varepsilon}$, with a negative slope directly reflecting the value of m^* [38]:

$$\Delta_+ = E_+ - \left(1 - \frac{m}{m^*}\right)\bar{\varepsilon}. \tag{1}$$

Our data indeed exhibit such a linear decrease of Δ_+ with increasing $\bar{\varepsilon}$ [see Figs. 2(b) and 2(c)].

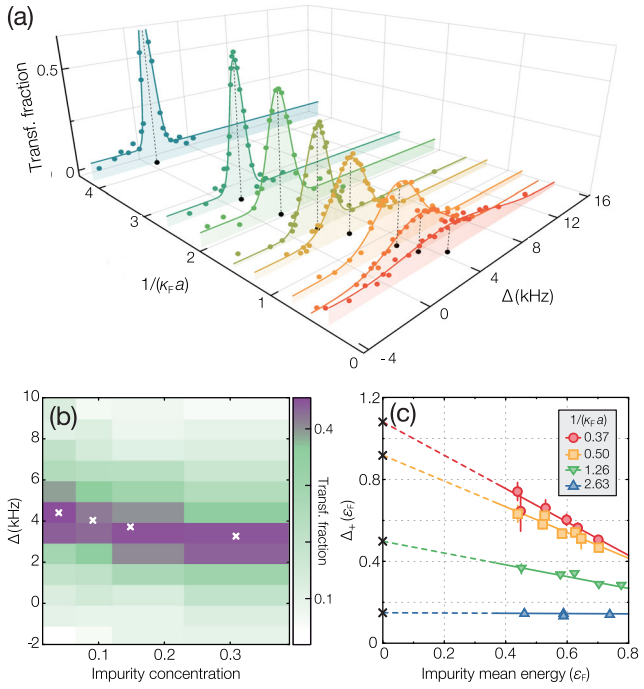

FIG. 2. Examples of the repulsive polaron spectral response recorded (a) at different $1/(\kappa_F a)$ values with concentration $x = 0.15(3)$ and (b) at different x values with $\kappa_F a \simeq 2$. (c) Resonance position Δ_+ as a function of $\bar{\varepsilon}$ for various $1/(\kappa_F a)$ values (see the legend). The linear fits used to extract E_+ and m/m^* are shown. Error bars denote the standard errors of the fitted Δ_+.

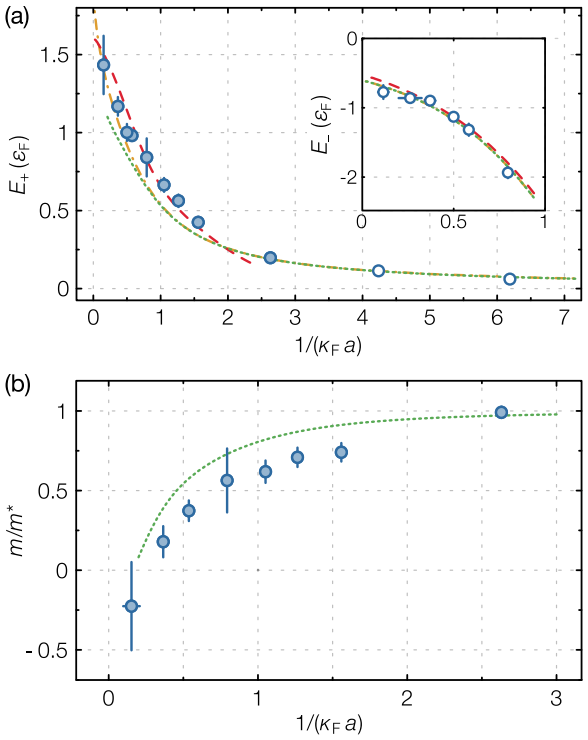

FIG. 3. (a) Zero-momentum repulsive polaron energy E_+ as a function of $1/(\kappa_F a)$ (symbols). Inset: Attractive polaron energy E_-. Theory predictions from Refs. [23] (dot-dashed yellow line), [25] (dotted green line), and [26] (dashed red line) are shown in both panels. Empty symbols denote points obtained by averaging measurements at different $\bar{\varepsilon}$ rather than by zero-energy extrapolation [38]. (b) Inverse effective mass m/m^* of the repulsive polaron as a function of $1/\kappa_F a$ (symbols), together with theory predictions from Ref. [25] (dotted green line). Error bars combine the linear fit parameter errors with the standard error of the mean (s.e.m.) of binned data.

On the other hand, polaron-polaron effective interactions are expected, within an equilibrium Fermi liquid, to contribute with a positive resonance shift $\propto x \sim \varepsilon^{3/2}$ [2,38,54,55], leading to a nonlinear increase of Δ_+ with $\bar{\varepsilon}$. Such a trend is incompatible with the observed linear decrease. Furthermore, sizable effective interactions would induce additional spectral broadening and decoherence [18] for increasing x, never exhibited by our data [see Fig. 2(b) and Ref. [38]]. Therefore, our measurements show no evidence of polaron interaction effects. In light of this, for all explored values of $\kappa_F a$, we extract the polaron energy E_+ and effective mass m^* by fitting our data with Eq. (1). In determining these quantities, we have also taken into account the weak initial interaction energy of state-$|2\rangle$ impurities in the state-$|1\rangle$ medium [see Fig. 1(a)] and the associated tiny mass renormalization [38].

The determined behaviors of E_+ and m/m^* are presented in Figs. 3(a) and 3(b), respectively. The polaron energy E_+ is found in good agreement with recent $T = 0$ theoretical predictions based either on a variational model [23], on diagrammatic calculations within the ladder approximation [25,38], or on the functional renormalization group [26], which in turn compare well to quantum Monte Carlo (QMC) simulations [24]. Importantly, for $1/(\kappa_F a) < 1/(\kappa_F a)_c = 1/1.7(2) \simeq 0.6(1)$, E_+ exceeds ε_F, indicating that the Fermi liquid of repulsive polarons becomes energetically disfavored against a phase-separated state [23–25]. This value of $(\kappa_F a)_c$ is larger than that recently reported for a balanced spin mixture [32], consistently with QMC predictions [24]. In the inset in Fig. 3(a), we also present the attractive polaron energy E_-, extracted by fitting the resonances at $\Delta < 0$ in the spectra recorded at strong interactions (see [38] for further details). Here, we find excellent agreement with theories and previous experiments [14,25,26,53].

The behavior of the repulsive polaron effective mass also provides important information: The extracted m/m^* strongly decreases for increasing $\kappa_F a$, until it becomes zero and eventually turns negative at very strong repulsion. This feature, never observed experimentally, has been previously pointed out in the context of attractive Fermi polarons [36,37]. There, a negative m^* has been predicted for interaction strengths well beyond the polaron-molecule crossing and interpreted as a signature for the attractive polaron being thermodynamically unstable against the dressed dimer. Similarly, the observation of $m^* < 0$ at $\kappa_F a > \kappa_F a_c$ suggests a thermodynamic instability of the repulsive Fermi liquid. Overall, the experimental trend of m^* is reasonably reproduced by the theory from Ref. [25] [see the line in

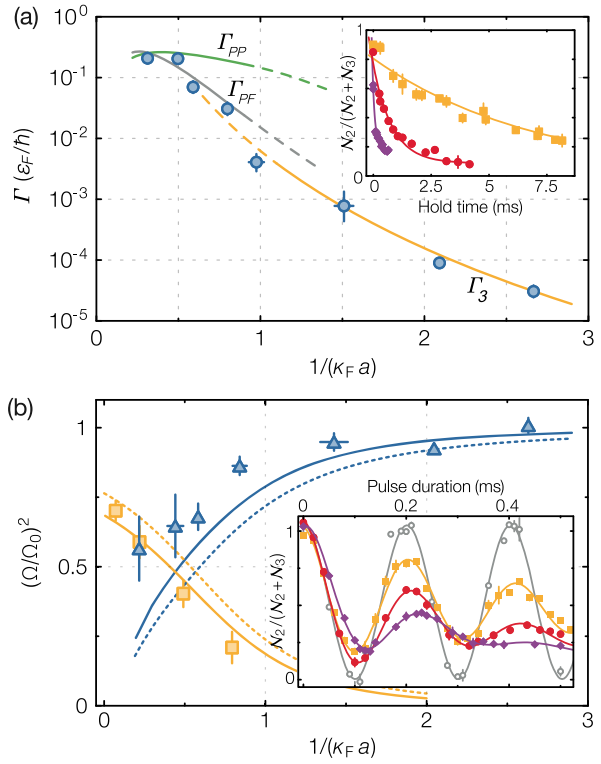

FIG. 4. (a) Decay rate Γ of the repulsive branch population measured as a function of $1/(\kappa_F a)$. Theory predictions for three-body recombination Γ_3 [56] (yellow line), polaron-to-polaron Γ_{PP} [25] (green line), and polaron-to-bare atom Γ_{PF} [38] (gray line) decay processes are plotted within their respective regimes of validity. Inset: Examples of polaron population decay for $\kappa_F a \simeq 1$ (yellow squares), 1.3 (red circles), and 3 (purple diamonds), together with the exponential fits. (b) $(\Omega/\Omega_0)^2$ for the repulsive (blue triangles) and attractive (yellow squares) polarons at various $1/(\kappa_F a)$. Solid curves are our theory predictions for $(\Omega/\Omega_0)^2$ obtained within the ladder approximation [38], while dotted curves depict the lowest-order results $\sqrt{Z_{+2}Z_{\pm 3}}$. Inset: Repulsive polaron Rabi oscillations at $x = 0.15(3)$ for $\kappa_F a \simeq 0$ (empty gray circles), 1.1 (yellow squares), 1.3 (red circles), and 1.7 (purple diamonds). Error bars combine the fit parameter errors with binned data s.e.m.

Fig. 3(b)], which is, however, expected to underestimate m^*, since it includes only one-particle-hole excitations [36].

After investigating the elastic properties of the repulsive polaron, we turn to consider its lifetime. This is a key quantity that sets the stability of the repulsive Fermi gas and the applicability of Landau's quasiparticle theory in its description. Following Ref. [17], we measure the quasiparticle decay rate through a double-pulse excitation scheme: A first π pulse initially transfers state-$|2\rangle$ atoms to the repulsive branch; a second pulse, identical to the first, selectively brings repulsive quasiparticles back to the weakly interacting state after a variable hold time. By fitting the relative state-$|2\rangle$ population measured as a function of time with an exponential decay, we extract the decay rate Γ of the repulsive quasiparticle branch for various interaction strengths. The results are summarized in Fig. 4(a). We do not observe any appreciable dependence of Γ upon concentration for $0.05 \leq x \leq 0.4$, and the data shown in Fig. 4 are collected setting $x = 0.15(1)$. Γ is found to strongly increase towards unitarity, spanning nearly 4 orders of magnitude in the range $1/(\kappa_F a) = 0.3 \ldots 2.7$.

At weak coupling $\kappa_F a < 1$, the polaron decay is well described by the three-body recombination at rate Γ_3 of bare impurities colliding with two fermions from the bath [56]. For $\kappa_F a > 1$, the medium starts playing an essential role: The bound-state energy is modified with respect to the one in vacuum, and alternative decay channels open up [10,38]. In particular, it has been predicted that the zero-momentum repulsive polaron lifetime is limited for strong interactions by rapid two-body inelastic decay onto attractive polarons, which represent the many-body ground state for $\kappa_F a \geq 1.15$. The two-body decay rate Γ_{PP}, calculated in the ladder approximation for such polaron-to-polaron decay processes [25], matches the data only close to unitarity while greatly underestimating the polaron lifetime for $1/(\kappa_F a) > 0.5$. In contrast, we recover a good quantitative agreement for a wider range of $\kappa_F a$ by considering bare particles, rather than attractive polarons, as final decay products in the calculation [38] [see the gray line in Fig. 4(a)]. In particular, we emphasize that the measured rate is about 20% of $\varepsilon_F/\hbar$ close to unitarity, and it is below 10% of $\varepsilon_F/\hbar$ at $1/(\kappa_F a)_c \simeq 0.6$, much smaller than theoretical expectations [25,26].

Finally, we probe the coherence properties of the repulsive polaron. As opposed to molecular excitations, polaron quasiparticles feature a coherent nature, usually quantified in terms of the quasiparticle residue Z [10], namely, the squared overlap between the noninteracting and the many-body polaron wave functions. Information on Z can be obtained either from spatially resolved rf spectra [14] or by driving Rabi oscillations on the free-to-polaron transition [17]. For a noninteracting initial state, $Z = (\Omega/\Omega_0)^2$, where Ω (Ω_0) is the Rabi frequency of the polaron quasiparticle (bare particle) state [17]. We modify this simple relation to account for the nonzero interactions of the initial $|2\rangle$ state with the bath and obtain predictions for $(\Omega/\Omega_0)^2$ [38]. Examples of repulsive polaron Rabi oscillations at various $1/(\kappa_F a)$ values are displayed in the inset in Fig. 4(b), where $\Omega_0 = 2\pi \times 4.95(5)$ kHz $\simeq 0.7\varepsilon_F/\hbar$. As $\kappa_F a$ is increased, the repulsive polaron Rabi frequency progressively decreases, accompanied by an increasing damping rate of the oscillations. Such damping is much faster than the corresponding quasiparticle decay, indicating that decoherence induced by elastic collisions, rather than inelastic relaxation processes, is the dominant damping mechanism [17,18,38]. Interestingly, the damping rate quantitatively matches the predicted quasiparticle peak spectral width [26,38]. The extracted $(\Omega/\Omega_0)^2$ from damped sinusoidal fits for both repulsive and attractive polarons are presented in Fig. 4(b), together with our theoretical predictions based on the ladder approximation [38].

In conclusion, we presented a thorough study of the elastic and inelastic properties of repulsive Fermi polarons for a mass-balanced highly polarized spin mixture at a broad Feshbach resonance. While further theoretical effort is required for a comprehensive description of our experimental data, we demonstrate repulsive quasiparticle lifetimes greatly exceeding $10\hbar/\varepsilon_F$ over a wide range of interactions, far longer than recent predictions [25,26]. We also show that repulsive polarons remain well-defined coherent excitations even at very strong coupling by observing Rabi oscillations up to $1/(\kappa_F a) \simeq 0.2$. Moreover, we reveal an interaction regime where the paramagnetic Fermi liquid becomes energetically and thermodynamically unstable, motivating future studies aimed at directly observing ferromagnetism in metastable repulsive Fermi gases. Finally, our spectroscopic protocol can be extended to balanced mixtures, opening up new perspectives for monitoring the dynamical growth of polarized domains after a fast, yet selective rf quench to the upper branch of the many-body system and the competing pairing instability [10,31–33].

We thank G. Bertaina, G. Bruun, X. Cui, T. Enss, O. Goulko, D. Petrov, S. Pilati, N. Prokof'ev, B. Svistunov, H. Zhai, and the LENS Quantum Gases group for useful discussions and R. Grimm and J. Levinsen for a critical reading of the manuscript. This work was supported by the ERC through Grants No. 307032 QuFerm2D and No. 637738 PoLiChroM and through the EU H2020 Marie Skłodowska-Curie program (Grant No. 705269 SCOUTFermi2D to F. S.). P. M. acknowledges funding from a "Ramón y Cajal" fellowship, from MINECO (Severo Ochoa SEV-2015-0522 and FOQUS FIS2013-46768), Generalitat de Catalunya (SGR 874), and the Fundació Privada Cellex.

Note added.—While completing the experimental measurements, we became aware of related theoretical work by Goulko *et al.* [57], in which diagrammatic Monte Carlo results are shown to be compatible with our data.

*scazza@lens.unifi.it

[1] L. Landau, Sov. Phys. JETP **3**, 920 (1957).
[2] J. Bardeen, G. Baym, and D. Pines, Phys. Rev. **156**, 207 (1967).
[3] J. M. D. Teresa, M. R. Ibarra, P. A. Algarabel, C. Ritter, C. Marquina, J. Blasco, J. Garcia, A. del Moral, and Z. Arnold, Nature (London) **386**, 256 (1997).
[4] A. J. Millis, Nature (London) **392**, 147 (1998).
[5] C. Deibel and V. Dyakonov, Rep. Prog. Phys. **73**, 096401 (2010).
[6] A. Davydov, J. Theor. Biol. **38**, 559 (1973).
[7] L. Radzihovsky and D. E. Sheehy, Rep. Prog. Phys. **73**, 076501 (2010).
[8] F. Chevy and C. Mora, Rep. Prog. Phys. **73**, 112401 (2010).
[9] M. Knap, A. Shashi, Y. Nishida, A. Imambekov, D. A. Abanin, and E. Demler, Phys. Rev. X **2**, 041020 (2012).
[10] P. Massignan, M. Zaccanti, and G. M. Bruun, Rep. Prog. Phys. **77**, 034401 (2014).
[11] C. Lobo, A. Recati, S. Giorgini, and S. Stringari, Phys. Rev. Lett. **97**, 200403 (2006).
[12] M. W. Zwierlein, A. Schirotzek, C. H. Schunck, and W. Ketterle, Science **311**, 492 (2006).
[13] G. B. Partridge, W. Li, R. I. Kamar, Y.-a. Liao, and R. G. Hulet, Science **311**, 503 (2006).
[14] A. Schirotzek, C.-H. Wu, A. Sommer, and M. W. Zwierlein, Phys. Rev. Lett. **102**, 230402 (2009).
[15] S. Nascimbène, N. Navon, K. J. Jiang, L. Tarruell, M. Teichmann, J. McKeever, F. Chevy, and C. Salomon, Phys. Rev. Lett. **103**, 170402 (2009).
[16] N. Navon, S. Nascimbène, F. Chevy, and C. Salomon, Science **328**, 729 (2010).
[17] C. Kohstall, M. Zaccanti, M. Jag, A. Trenkwalder, P. Massignan, G. M. Bruun, F. Schreck, and R. Grimm, Nature (London) **485**, 615 (2012).
[18] M. Cetina, M. Jag, R. S. Lous, I. Fritsche, J. T. M. Walraven, R. Grimm, J. Levinsen, M. M. Parish, R. Schmidt, M. Knap, and E. Demler, Science **354**, 96 (2016).
[19] M. Koschorreck, D. Pertot, E. Vogt, B. Fröhlich, M. Feld, and M. Köhl, Nature (London) **485**, 619 (2012).
[20] J. Catani, G. Lamporesi, D. Naik, M. Gring, M. Inguscio, F. Minardi, A. Kantian, and T. Giamarchi, Phys. Rev. A **85**, 023623 (2012).
[21] M.-G. Hu, M. J. Van de Graaff, D. Kedar, J. P. Corson, E. A. Cornell, and D. S. Jin, Phys. Rev. Lett. **117**, 055301 (2016).
[22] N. B. Jørgensen, L. Wacker, K. T. Skalmstang, M. M. Parish, J. Levinsen, R. S. Christensen, G. M. Bruun, and J. J. Arlt, Phys. Rev. Lett. **117**, 055302 (2016).
[23] X. Cui and H. Zhai, Phys. Rev. A **81**, 041602(R) (2010).
[24] S. Pilati, G. Bertaina, S. Giorgini, and M. Troyer, Phys. Rev. Lett. **105**, 030405 (2010).
[25] P. Massignan and G. Bruun, Eur. Phys. J. D **65**, 83 (2011).
[26] R. Schmidt and T. Enss, Phys. Rev. A **83**, 063620 (2011).
[27] P. Massignan, Z. Yu, and G. M. Bruun, Phys. Rev. Lett. **110**, 230401 (2013).
[28] R. A. Duine and A. H. MacDonald, Phys. Rev. Lett. **95**, 230403 (2005).
[29] S.-Y. Chang, M. Randeria, and N. Trivedi, Proc. Natl. Acad. Sci. U.S.A. **108**, 51 (2011).
[30] G.-B. Jo, Y.-R. Lee, J.-H. Choi, C. A. Christensen, T. H. Kim, J. H. Thywissen, D. E. Pritchard, and W. Ketterle, Science **325**, 1521 (2009).
[31] C. Sanner, E. J. Su, W. Huang, A. Keshet, J. Gillen, and W. Ketterle, Phys. Rev. Lett. **108**, 240404 (2012).
[32] G. Valtolina, F. Scazza, A. Amico, A. Burchianti, A. Recati, T. Enss, M. Inguscio, M. Zaccanti, and G. Roati, arXiv:1605.07850.
[33] D. Pekker, M. Babadi, R. Sensarma, N. Zinner, L. Pollet, M. W. Zwierlein, and E. Demler, Phys. Rev. Lett. **106**, 050402 (2011).
[34] S. Gupta, Z. Hadzibabic, M. W. Zwierlein, C. A. Stan, K. Dieckmann, C. H. Schunck, E. G. M. van Kempen, B. J. Verhaar, and W. Ketterle, Science **300**, 1723 (2003).
[35] C. A. Regal and D. S. Jin, Phys. Rev. Lett. **90**, 230404 (2003).
[36] R. Combescot, S. Giraud, and X. Leyronas, Europhys. Lett. **88**, 60007 (2009).
[37] C. Trefzger and Y. Castin, Phys. Rev. A **85**, 053612 (2012).

[38] See Supplemental Material at http://link.aps.org/supplemental/10.1103/PhysRevLett.118.083602 for experimental and theoretical methods, and details on attractive polaron measurements and collisional decoherence, which includes Refs. [39–52].
[39] A. Burchianti, G. Valtolina, J. A. Seman, E. Pace, M. De Pas, M. Inguscio, M. Zaccanti, and G. Roati, Phys. Rev. A **90**, 043408 (2014).
[40] G. Zürn, T. Lompe, A. N. Wenz, S. Jochim, P. S. Julienne, and J. M. Hutson, Phys. Rev. Lett. **110**, 135301 (2013).
[41] R. Bishop, Ann. Phys. (N.Y.) **78**, 391 (1973).
[42] F. Chevy, Phys. Rev. A **74**, 063628 (2006).
[43] S. Pilati and S. Giorgini, Phys. Rev. Lett. **100**, 030401 (2008).
[44] Z. Yu, S. Zöllner, and C. J. Pethick, Phys. Rev. Lett. **105**, 188901 (2010).
[45] R. J. Fletcher, R. Lopes, J. Man, N. Navon, R. P. Smith, M. W. Zwierlein, and Z. Hadzibabic, arXiv:1608.04377.
[46] J. Vlietinck, J. Ryckebusch, and K. Van Houcke, Phys. Rev. B **87**, 115133 (2013).
[47] C. Trefzger and Y. Castin, Europhys. Lett. **101**, 30006 (2013).
[48] R. Combescot, A. Recati, C. Lobo, and F. Chevy, Phys. Rev. Lett. **98**, 180402 (2007).
[49] P. Massignan, G. M. Bruun, and H. T. C. Stoof, Phys. Rev. A **77**, 031601(R) (2008).
[50] M. M. Parish and J. Levinsen, Phys. Rev. B **94**, 184303 (2016).
[51] I. I. Sobelman, *An Introduction to the Theory of Atomic Spectra* (Pergamon, Oxford, 1972).
[52] M. Cetina, M. Jag, R. S. Lous, J. T. M. Walraven, R. Grimm, R. S. Christensen, and G. M. Bruun, Phys. Rev. Lett. **115**, 135302 (2015).
[53] N. Prokof'ev and B. Svistunov, Phys. Rev. B **77**, 020408 (2008).
[54] C. Mora and F. Chevy, Phys. Rev. Lett. **104**, 230402 (2010).
[55] Z. Yu and C. J. Pethick, Phys. Rev. A **85**, 063616 (2012).
[56] D. S. Petrov, Phys. Rev. A **67**, 010703 (2003).
[57] O. Goulko, A. S. Mishchenko, N. Prokof'ev, and B. Svistunov, Phys. Rev. A **94**, 051605(R) (2016).